Flow Measurement and Instrumentation 81 (2021) 102025

Contents lists available at ScienceDirect

Flow Measurement and Instrumentation

journal homepage: www.elsevier.com/locate/flowmeasinst

Thermal boundary layers in critical flow venturis

John D. Wright [a,*], Woong Kang [b], Aaron N. Johnson [a], Vladimir B. Khromchenko [a], Michael R. Moldover [a], Liang Zhang [c], Bodo Mickan [d]

[a] National Institute of Standards and Technology (NIST), 100 Bureau Drive, Gaithersburg, MD, 20899, USA
[b] Korea Research Institute of Standards and Science (KRISS), South Korea
[c] National Institute of Metrology–China (NIM), China
[d] Physikalisch Technische Bundesanstalt (PTB), Germany

ARTICLE INFO

Keywords:
Critical flow venturi
Thermal boundary layer
Discharge coefficient

ABSTRACT

We improve the usefulness of small (diameter < 10 mm) critical flow venturis (CFVs) as transfer standards for gas flow by measuring and explaining how their discharge coefficients depend on the temperature T of their environment. At Reynolds numbers $Re < 2.5 \times 10^5$ (e.g., a 2 mm diameter throat; inlet air at 1 MPa), CFVs exhibit sensitivity to the environmental temperature of approximately 0.02 % K^{-1} due to biased measurements of the stagnation temperature T_0 (temperature "sampling" error) and from ignoring the low-density, annular, thermal boundary layer generated by heat transfer from the CFV's body to the gas flowing through the CFV. To reduce temperature sampling errors, we used a non-metallic approach pipe and a temperature sensor with a low stem-conduction error. To correct for thermal boundary layer effects on the flow, we used Geropp's functional form: $C_T = 1 + K_T \mathrm{Re}^{-1/2}[\Delta T/T_0]$ where ΔT is the difference between the CFV's inner wall temperature and the stagnation temperature. For CFVs made of stainless steel and copper with diameters of $d = 0.56$ mm, 1.1 mm, and 3.2 mm we measured $K_T \approx -7$ while theoretical predictions of K_T by Geropp and Ding et al. are −1.7 and −3.845 respectively. Introducing the correction for room temperature changes (C_T) measured in this work, reduces the room temperature sensitivity of the flow measured with the 0.56 mm diameter CFVs from 0.02 % K^{-1} to less than 0.003 % K^{-1}. Smaller, but significant, improvements are achieved with larger CFVs.

1. Introduction to critical flow venturis

Toroidal critical flow venturis (CFVs) consistent with documentary standards have a contracting inlet with a radius of curvature approximately twice the throat diameter followed by a conical outlet. If a sufficiently large pressure ratio is maintained across the CFV (conservatively $P_{up}/P_{down} > 2$ for air), the gas entering the CFV expands and reaches sonic velocity at the throat. The commonly used "0th order" physical model assumes isentropic flow and adiabatic wall conditions to calculate mass flow $\dot{m}_{R*}$ from the upstream stagnation pressure P_0 and temperature T_0:

$$\dot{m}_{R*} = C_R^* \frac{P_0 A_{ref} \sqrt{M}}{\sqrt{R T_0}} \tag{1}$$

where $A_{ref} = \pi d_{ref}^2/4$ is the throat area, C_R^* is the real critical flow factor (calculated from a thermodynamic database [1]),[1] M is the gas molar mass, and R is the universal gas constant [2]. More details about the geometry of CFVs and the commonly used flow model can be found in documentary standards [3,4].

A discussion of nomenclature is useful at this point. The literature about CFVs often defines a discharge coefficient C_d as the ratio of a measured reference flow $\dot{m}_{ref}$ to a calculated CFV flow $\dot{m}_{CFV}$,

$$C_d = \frac{\dot{m}_{ref}}{\dot{m}_{CFV}} \tag{2}$$

However, this definition of C_d is not unique because it does not specify which model should be used to calculate $\dot{m}_{CFV}$. Herein, we will represent corrections for the various effects using the following subscripts: 1) **R*** for the real gas property effects [1], 2) **inv** for the inviscid core flow effects, 3) **vbl** for the velocity boundary layer effects with an adiabatic wall, 4) $\boldsymbol{\alpha}$ for the effects of throat thermal expansion, and 5) **tbl** or **T** for thermal boundary layer effects resulting from heat transfer from

* Corresponding author.
E-mail address: john.wright@nist.gov (J.D. Wright).

[1] Note that the ideal critical flow factor C_I^* (calculated from the gas specific heat ratio as a function of pressure and temperature) is sometimes used but C_R^* better accounts for real gas effects.

https://doi.org/10.1016/j.flowmeasinst.2021.102025
Received 29 June 2021; Received in revised form 1 July 2021; Accepted 26 July 2021
Available online 30 July 2021
0955-5986/

Nomenclature:

$A_{\mathrm{ref}} = \pi d_{\mathrm{ref}}^{2}/4$	Critical flow venturi (CFV) throat area at reference temperature
$Bi = h\ell/k$	Biot number, ratio of convective to conductive heat flux resistance
$C_{\mathrm{d}} = \dot{m}_{\mathrm{ref}}/\dot{m}_{\mathrm{CFV}}$	Experimental CFV discharge coefficient
C_{inv}	Correction to CFV 0$^{\mathrm{th}}$ order model for the inviscid, core flow
C_{tbl}	Theoretical correction to account for heat transfer between the thermal boundary layer and an isothermal CFV wall
C_{T}	Experimental correction to CFV 0$^{\mathrm{th}}$ order model for the thermal boundary layer relative to a CFV wall at a reference temperature condition
C_{α}	Correction to CFV 0$^{\mathrm{th}}$ order model for throat thermal expansion
C_{vbl}	Correction to CFV 0$^{\mathrm{th}}$ order model for the velocity boundary layer with an adiabatic wall condition
C_{R}^{*}	Real gas critical flow factor (calculated from a thermodynamic database)
d_{ref} or d	CFV throat diameter at reference temperature
h	Convective heat transfer coefficient at the CFV interior wall
k	Material thermal conductivity
ℓ	Distance from the CFV interior wall to the CFV exterior wall
$K_{\mathrm{T}}, K_{\mathrm{tbl}}$	Dimensionless proportionality constant between $Re^{-1/2}(\Delta T)/T_0$ and C_{tbl} or C_{T}
M	Gas molar mass
Ma	Mach number
$\dot{m}_{\mathrm{R}*} = C_{\mathrm{R}}^{*} P_0 A_{\mathrm{ref}} \sqrt{M}/\sqrt{RT_0}$	0$^{\mathrm{th}}$ order CFV mass flow, accounting only for real gas effects
$\dot{m}_{\mathrm{ref}}$	Mass flow measured with a reference flow standard
$\dot{m}_{\mathrm{CFV}}$	Mass flow through a CFV calculated by theoretical or analytical means
P_0	Stagnation pressure at the CFV approach-pipe.
Pr	Prandtl number
$Re = \frac{4\dot{m}}{\pi d \mu_0}$	Reynolds number, using the throat diameter as length scale, μ_0 is the dynamic viscosity based on P_0 and T_0
R	Universal gas constant
R_c	Radius of curvature of the CFV inlet near the throat
s	CFV shape parameter
T_0	Stagnation temperature in the CFV approach-pipe.
T_{aw}	CFV wall temperature assuming an adiabatic condition between the wall and the flowing gas
T_{body}	CFV body temperature
T_{core}	Temperature of the core flow
T_{ref}	Reference temperature used for the throat dimensions and isothermal CFV wall
T_{room}	Room temperature
T_{wall}	CFV interior wall temperature
T_{surf}	CFV exterior wall temperature
ΔT	$T_{\mathrm{wall}} - T_0 \approx T_{\mathrm{body}} - T_0$
T_z	Temperature measured at axial position $z = 10$ mm upstream from CFV inlet
α	Linear coefficient of thermal expansion for the CFV body material
δ^{*}	Boundary layer displacement thickness
γ	Ratio of the constant pressure to constant volume specific heats $= c_P/c_V$
Ω	CFV throat curvature ratio, $= d/(2R_c) \approx 0.25$ for standard CFV geometry

the CFV wall to the flowing gas. In this nomenclature, $\dot{m}_{\mathrm{R}*,\ \mathrm{inv,\ vbl,\ tbl,}\ \alpha} = C_{\mathrm{inv}} C_{\mathrm{vbl}} C_{\mathrm{tbl}} C_{\alpha}\ \dot{m}_{\mathrm{R}*}$. In prior CFV publications, C_{d} usually represents $C_{\mathrm{inv}} C_{\mathrm{vbl}} C_{\mathrm{tbl}}$ measured at room temperature. In this publication, we will avoid using C_{d}; instead, we will use more specific notation such as $C_{\mathrm{inv}} C_{\mathrm{vbl}} C_{\mathrm{tbl}} C_{\alpha}$ where the subscripts identify the phenomena included in the theoretical mass flow calculations.

Most users calibrate their CFV against a reference flow standard over a range of P_0 values and apply an experimentally measured discharge coefficient $\dot{m}_{\mathrm{ref}}/\dot{m}_{\mathrm{R}*}$. Alternatively, if the CFV inlet shape and throat diameter are well known, analytical calculations of the corrections C_{inv} and C_{vbl} give excellent agreement with experimental calibration data (except near the laminar-to-turbulent transition of the velocity boundary layer). Hall in 1962 [5] and Kliegel and Levine in 1969 [6] calculated inviscid core flow corrections (C_{inv}) that reduce the 0$^{\mathrm{th}}$ order mass flow for the standard-shaped CFV by 0.12 % for all CFV sizes and flows. For small CFVs, the departure from the 0$^{\mathrm{th}}$ order model is primarily due to the thickness of the velocity boundary layer at the wall: the lower velocities in the boundary layer reduce the mass flux relative to the assumption of sonic velocity across the entire throat. Tang in 1969 [7] and Geropp in 1971 [8] used similarity transformations to calculate corrections for the laminar boundary layer effects for an adiabatic wall and Prandtl-number $Pr = 1$ (C_{vbl}). Low-uncertainty dimensional and flow measurements have confirmed that the analytically-calculated values of $C_{\mathrm{inv}} C_{\mathrm{vbl}}$ for the laminar flow regime are correct within 0.05 % [9,10]. Similar agreement could be obtained in comparison with alternative numerical solutions based on the momentum differential equation of the boundary layer using integral methods [11,12].

In this study, the boundary layer is laminar because the Reynolds numbers are all less than 1×10^6, the value where the transition from laminar to turbulent flow normally occurs in CFVs. Because the laminar boundary layer thickness scales with $Re^{-1/2}$, measured values of $\dot{m}_{\mathrm{ref}}/\dot{m}_{\mathrm{R}*,\ \mathrm{inv,\ vbl,\ tbl}}$ are a nearly-linear function of $Re^{-1/2}$. Because the interactions between the various phenomena (C_{inv}, C_{vbl}, etc.) are weak, we use Composite Linear CFV theory [9] and simply multiply correction ratios from various sources to calculate their combined effect, thereby neglecting interactions of phenomena.

2. Introduction to thermal effects on CFVs

CFVs are often used as working standards to calibrate other meters or as transfer standards during inter-laboratory comparisons because of 1) their excellent calibration stability over time [13], and 2) the well-developed physical model that accounts for their sensitivity to gas properties and to the gas temperature. However, smaller CFVs ($d < 10$ mm) show significant, unaccounted sensitivity to the temperature of the CFV's environment. During the CCM.FF-K6 2002 key comparison, the temperature sensitivity of the CFV transfer standard accounted for 40 % of the uncertainty contributed by the transfer standard at the lower flows [14].

Fig. 1 shows a 5-fold error reduction in CFV flow measurements when the thermal-effect correction C_{T} described below is applied to a $d = 0.56$ mm CFV. It shows the change in CFV mass flow relative to a very accurate (0.03 % uncertainty[2]) reference flow measurement when room temperature (T_{room}) was changed from 296 K to 303 K and back to 296 K. Using the normal approach to calculate flow through the CFV ($\dot{m}_{\mathrm{CFV}} = C_{\mathrm{inv}} C_{\mathrm{vbl}}\ \dot{m}_{\mathrm{R}^*}$), the 7 K room temperature change leads to a flow measurement error of 0.12 %. Correcting for thermal expansion of the

[2] All uncertainties are approximately 95 % confidence level.

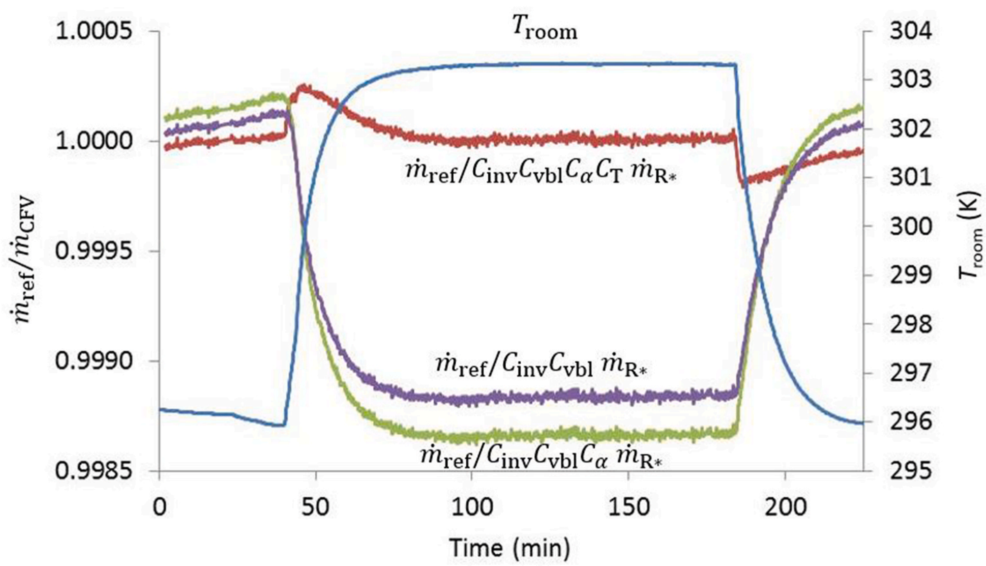

Fig. 1. Time dependence of the room temperature (T_{room}; right-hand scale) and the flows calculated using three flow models for a 0.56 mm diameter CFV. The data labelled $\dot{m}_{ref}/C_{inv}C_{vbl}\ \dot{m}_{R*}$ and $\dot{m}_{ref}/C_{inv}C_{vbl}C_{\alpha}\ \dot{m}_{R*}$ represent normal CFV flow calculations based on room temperature calibrations. The data labelled $\dot{m}_{ref}/C_{inv}C_{vbl}C_{\alpha}C_T\ \dot{m}_{R*}$ are nearly independent of T_{room} thereby demonstrating the effectiveness of the correction C_T developed in this work. During steady state temperature conditions, using C_T reduces the room temperature effect from approximately 0.02 % K^{-1} to a negligible level.

CFV material ($\dot{m}_{CFV} = C_{inv}C_{vbl}C_{\alpha}\ \dot{m}_{R*}$) increases the flow measurement error to 0.14 % (0.02 % K^{-1}). By introducing a correction for thermal boundary layer effects ($\dot{m}_{CFV} = C_{inv}C_{vbl}C_{\alpha}C_T\dot{m}_{R*}$), the errors are < 0.003 %, except during the periods of rapidly changing room temperature where they are as large as 0.025 %.

Early studies of thermal effects on CFVs used relatively large CFVs ($d \approx 25$ mm) where thermal boundary layer effects are not significant because the thermal boundary layer comprised a negligible fraction of the throat area [15–17]. The researchers were interested in the temperature profile within the CFV's body and the best location to measure the CFV body temperature to account for the thermal expansion of the throat area. More recently, Bignell and Choi [18] measured thermal boundary layer effects using smaller CFVs that were comparable to the ones used in this work. They measured the dependence of the CFV flow on the CFV body temperature. As shown in Fig. 13, our results are similar to, but not identical with, those of Bignell and Choi.

For CFVs operating in the laminar regime (generally $d < 10$ mm), Wright [14] listed 4 sources of CFV temperature sensitivity in order of increasing importance: 1) sensitivity of reference sensors to T_{room}, *e.g.* the mass flow reference and the pressure sensor measuring P_0, 2) thermal expansion of the throat area, 3) the thermal boundary layer, and 4) temperature "sampling errors".

1) Reference sensor sensitivity: For our measurements, the pressure transducer was maintained within 297.3 K ± 0.3 K and had negligible (<0.01 %) sensitivity to temperature fluctuations. The reference flow standards (the 34 L and 677 L pressure-volume-temperature-time (*PVTt*) standards [19]) were in a temperature-controlled water bath and also had negligible temperature sensitivity.

2) Thermal expansion of the CFV throat area: The correction for unconstrained thermal expansion of the CFV throat is:

$$C_{\alpha} = \frac{A}{A_{ref}} = 1 + 2\,\alpha\left(T_{body} - T_{ref}\right) \tag{3}$$

where A_{ref} is the throat area at the reference temperature $T_{ref} = 298.15$ K, α is the linear coefficient of thermal expansion of the CFV material, and T_{body} is the measured temperature of the CFV. The fractional thermal expansion coefficient of the throat area was $2\,\alpha = 34 \times 10^{-6}\ K^{-1}$ for both the stainless steel (SS) and the Cu–Te alloy 145 CFVs we used in this study; it was $9 \times 10^{-6}\ K^{-1}$ for the machinable ceramic also used to make CFVs in this study. For the small CFVs in this study (d < 3.2 mm), thermal boundary layer effects are 5 times larger than the thermal expansion effect. Nevertheless, we applied the correction C_{α} to our data in order to isolate thermal boundary layer effects.

Ding et al. [20] proposed that literature values for the thermal expansion coefficients of the CFV materials do not apply for the experiments described later in this paper. Instead, they used a finite-element model to study the temperature dependence of the throat diameter. They assumed that the length of the CFV between the O-rings shown in Fig. 8 was held constant by the fiberglass-filled polytetrafluoroethylene (PTFE) cylinders. They found that for some of the CFVs, the throat diameter decreased with increasing temperature (*i.e.*, a *negative* value for α was appropriate). We also performed finite-element simulations using COMSOL[3] and obtained results similar to Ding et al. when we made the constrained-length assumption. However, the constrained-length assumption is not realistic. We measured the force applied to the flexible O-rings by using a torque wrench on the nuts that squeezed the O-rings; it was approximately 3 kN. After replacing the constrained-length assumption with a 3 kN force, our simulation results were essentially in agreement with Eq. (3). Specifically, the impact on the experimental values of the thermal boundary layer correction were <0.01 %. Therefore, we used Equation (3) to account for the thermal expansion of the CFVs described in this paper.

3) Thermal boundary layer: Warmer, lower density gas near the CFV wall reduces mass flux through the CFV, an effect that increases in significance at lower Reynolds numbers encountered when using smaller CFVs.

4) Temperature sampling errors: Ideally, we would measure the temperature of the gas averaged over the converging inlet plane of the CFV. Unfortunately, it is impractical to place a temperature sensor at the entrance to a small CFV, either because it disrupts the flow field or because it is so small that the sensor would be too fragile. CFV documentary standards [3,4] call for the temperature sensor to be placed approximately two approach-pipe diameters upstream from the CFV entrance plane. This work demonstrates that better-designed temperature measurements will yield more accurate flow measurements for small CFVs.

[3] In order to describe materials and procedures adequately, it is occasionally necessary to identify commercial products by manufacturers' name or label. In no instance does such identification imply endorsement by the National Institute of Standards and Technology, nor does it imply that the particular product or equipment is necessarily the best available for the purpose.

Fig. 2 illustrates the components of the CFV system and the heat fluxes between them that cause temperature sampling errors. The gas cools as it accelerates through the CFV and the gas cools the CFV body (path 1 in Fig. 2). The CFV body cools the approach-pipe and the inlet gas (paths 2). The temperature sensor used to measure T_0 can be in error due to stem conduction from the approach-pipe and the room temperature (paths 3). Changes in the room temperature and ventilation will lead to time-dependent and space-dependent heat fluxes on every component (paths 4). The temperature of the gas changes as it flows from the measurement point (T_0 sensor) to the inlet of the CFV. The thermal time response of the entire CFV system (including the temperature sensor) determines either 1) how long one must wait to perform a steady state flow measurement or 2) the bias of dynamic CFV flow measurements [21].

In the remainder of this paper we will 1) review Geropp's 1987 analytical solution for the non-adiabatic wall condition and propose a correction for thermal boundary layer effects, 2) discuss the temperature distribution within the CFV body and how we obtained approximate measurements of the interior wall temperature, 3) describe a custom CFV holder and approach-pipe design that reduced temperature sampling errors in our experiment to <0.02 %, and 4) present the results of experiments in which CFV bodies made of copper, stainless steel, and ceramic were heated to four set-point temperatures to quantify thermal boundary layer effects. Our objective is to present a physical model for a thermal boundary layer correction C_T to correct for temperature effects and thereby reduce the uncertainty of CFV gas flow measurements.

3. Geropp's similarity solution for the non-adiabatic boundary layer

The adiabatic wall assumed in Tang's 1969 [7] and Geropp's 1971 [8] solutions for the CFV boundary layer is a simplifying approximation. In most applications, the gas flowing along the wall of a thermally conductive CFV is warmer than gas near the wall of a thermally insulating (adiabatic) CFV. For $Re < 10^6$, there is a significant heat flux from the CFV body into a thermal boundary layer (Fig. 3). The thermal boundary layer is warmer than the free stream (or core flow) and its lower density leads to less mass flux through the CFV and hence smaller $\dot{m}_{\mathrm{ref}}/\dot{m}_{\mathrm{R*,\ inv,\ vbl,}\ \alpha}$ values.

In 1987, Geropp extended his similarity solution for the adiabatic CFV boundary layer [8] to include heat transfer between the CFV wall and the gas flow [22]. For simplicity, we assumed the Prandtl number (and hence the recovery factor) equals unity in the following summary

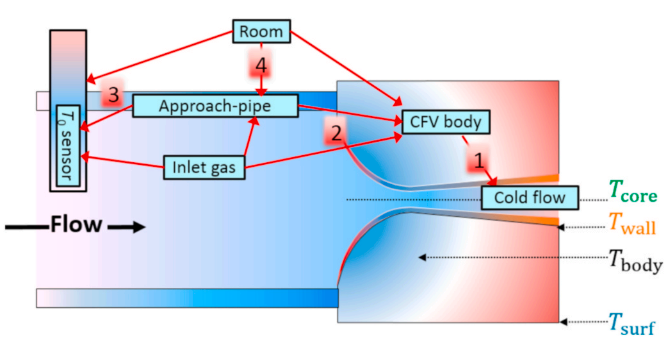

Fig. 2. Measured T_0 is subject to sampling errors due to heat transfer within the flow, CFV body, and approach-pipe walls. Numbered arrows indicate typical directions of heat flux between components.

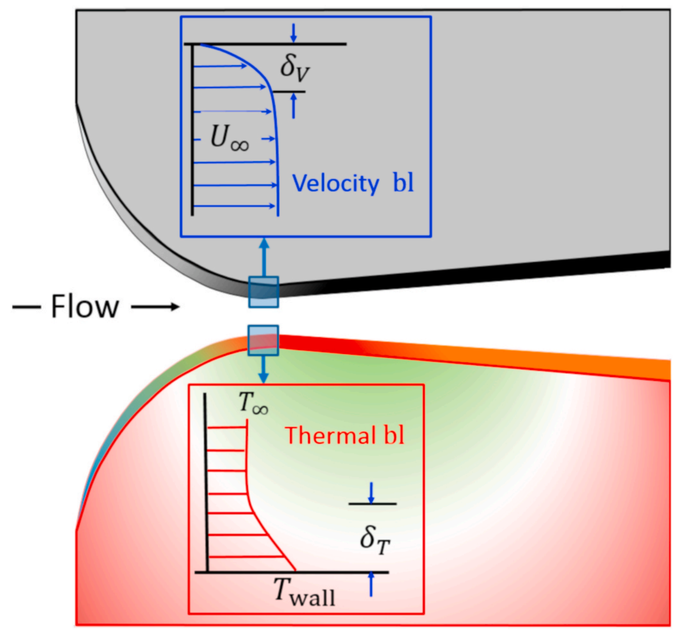

Fig. 3. Schematic representation of the velocity and thermal boundary layers in a critical flow venturi.

of Geropp's analysis. Equation (46) of Geropp '87 gives the displacement thickness[4] of the boundary layer at the CFV throat divided by the throat diameter:

$$\frac{\delta^*}{d} = (s\,Re)^{-1/2}\left[\frac{\gamma+1}{2}\right]^{\frac{1}{2(\gamma-1)}}\Psi \tag{4}$$

where:

$$\Psi = \sqrt{6}\left[1+\left(\frac{\gamma+1}{2}\right)\frac{\Delta T}{T_0}\right]\left(\sqrt{3+\frac{3}{2}\frac{\Delta T}{T_0}}-\sqrt{2+\frac{3}{2}\frac{\Delta T}{T_0}}\right)+ \\ +\frac{\sqrt{6}}{3}\left(\frac{\gamma-1}{2}\right)\left[\left(1+3\frac{\Delta T}{T_0}\right)\sqrt{2+\frac{3}{2}\frac{\Delta T}{T_0}}-3\frac{\Delta T}{T_0}\sqrt{3+\frac{3}{2}\frac{\Delta T}{T_0}}\right] \tag{5}$$

where $\gamma = c_P/c_V$, is the gas specific heat ratio, s is a CFV "shape parameter", and $\Delta T = T_{\mathrm{wall}} - T_0$ is the difference between the CFV's wall temperature and the stagnation temperature. The shape parameter is:

$$s = 2\sqrt{\Omega}\left(\frac{2}{\gamma+1}\right)^{\frac{1-3\gamma}{2(\gamma-1)}} \tag{6}$$

where Ω is the throat curvature ratio $= d/(2R_c)$ and R_c is the radius of curvature of the CFV inlet near the throat.

For a given gas species (γ), CFV geometry (d and Ω), and temperatures (T_0 and T_{wall}), Equations 4 through 6 allow one to calculate the product of the corrections for the velocity boundary layer and the non-adiabatic thermal boundary layer, $C_{\mathrm{vbl}}C_{\mathrm{tbl}}$:

$$C_{\mathrm{vbl}}C_{\mathrm{tbl}} = \frac{\left[\pi(d-2\delta^*)^2/4\right]}{\left[\pi d^2/4\right]} = 1-4\frac{\delta^*}{d}+4\left(\frac{\delta^*}{d}\right)^2 \cong 1-4\frac{\delta^*}{d} \tag{7}$$

For $\Delta T/T_0 = 0$, Geropp's 1987 solution simplifies to his 1971 adiabatic solution (for which $C_{\mathrm{tbl}} = 1$) and the first order expression for C_{vbl} is:

[4] Displacement thickness is the distance that the CFV wall would have to be moved towards the centerline to produce the same flow if the fluid was inviscid and had no boundary layer.

$$C_{\mathrm{vbl}} \cong 1-4\frac{\delta^*}{d}=1-4\,(s\,Re)^{-1/2}\left[\frac{\gamma+1}{2}\right]^{\frac{1}{2(\gamma-1)}}\Psi_0 \tag{8}$$

where $\Psi_0 = 3\sqrt{2}-2\sqrt{3}+\frac{(\gamma-1)}{\sqrt{3}}$. Note that the adiabatic wall solutions for C_{vbl} by Tang and Geropp do not ignore the existence of a thermal boundary layer; instead, their boundary layers are heated only by viscous dissipation of the flowing gas and not by heat transfer from the wall. Geropp's 1987 solution and the first order approximation in Equation (7) give:

$$C_{\mathrm{tbl}}=\frac{\text{isothermal wall}}{\text{adiabatic wall}}=\frac{Geropp\ \text{'87}(\Delta T\neq 0)}{Geropp\ \text{'87}(\Delta T=0)}=\frac{C_{\mathrm{vbl}}C_{\mathrm{tbl}}}{C_{\mathrm{vbl}}}$$

$$\cong \frac{1-4\,(s\,Re)^{-1/2}\left[\frac{\gamma+1}{2}\right]^{\frac{1}{2(\gamma-1)}}\Psi}{1-4\,(s\,Re)^{-1/2}\left[\frac{\gamma+1}{2}\right]^{\frac{1}{2(\gamma-1)}}\Psi_0} \tag{9}$$

First order Taylor's series expansions of Equation (9) around $Re^{-1/2}=0$ and $\Delta T/T_0=0$ lead to:

$$C_{\mathrm{tbl}} \cong 1+K_{\mathrm{tbl}}Re^{-1/2}\left[\frac{\Delta T}{T_0}\right] \tag{10}$$

where:

$$K_{\mathrm{tbl}}=\frac{\partial^2 C_{\mathrm{tbl}}}{\partial(Re^{-1/2})\partial\left(\frac{\Delta T}{T_0}\right)}=\frac{-2\sqrt{6}}{\sqrt{s}}\left(\frac{\gamma+1}{2}\right)^{\frac{1}{2(\gamma-1)}}$$

$$\left[\frac{\sqrt{3}}{2}-\frac{3}{2\sqrt{2}}+\frac{(\gamma-1)}{6\sqrt{2}}+2\left(\sqrt{3}-\sqrt{2}\right)\right] \tag{11}$$

The form of Equation (10) arises from the similarity solution of Geropp and matches our physical intuition: the thermal boundary layer thickness scales with $Re^{-1/2}$ [23] and the density change of the gas in the thermal boundary layer scales with $\Delta T/T_0$. Thermal boundary layer effects are larger for gases with large specific heat ratios: large γ causes lower free stream temperature T_{core} and therefore increased heat transfer from the CFV wall. C_{tbl} is also a function of the CFV inlet curvature ratio Ω: larger inlet curvature will lead to a thicker thermal boundary layer at the throat and smaller C_{tbl} values.

We also have applied Geropp's analysis without assuming a Prandtl number of unity to assess the sensitivity of K_{tbl} to the Prandtl number. For the standard CFV geometry and air used in our experiments (Ω = 0.25 and γ_{air} = 1.4), K_{tbl} = -2.2 for Prandtl number Pr = 1 and K_{tbl} = -1.7 for a Prandtl number Pr = 0.72 (the value for air).

In 2018, Ding et al. [20] also published a similarity solution for the thermal boundary layer in a CFV and obtained an equation similar in form to Geropp. However, their solution leads to a value of K_{tbl} = -3.845 for air.

4. Correcting thermal boundary layer effects in CFVs C_T

Geropp's theory accounts for thermal boundary layer effects in CFVs. We now consider a practical approach for applying Geropp's theory, particularly in situations where CFV users have neither accurate values for the CFV's geometry (d and Ω) nor values for the CFV's wall temperature T_{wall}. The need for accurate values of d and Ω can be circumvented by calibrating CFVs using a reference flow standard. Also T_{wall} of a typical metal CFV can be well approximated by the CFV's body temperature (See Section 5.). Because we cannot realize a truly adiabatic condition, we could not measure C_{tbl}; however, we will develop a correction for thermal boundary layer effects relative to a reference temperature condition.

Geropp's analysis suggests a practical approach to correcting for thermal boundary layer effects: calibrate a CFV against a flow reference at various wall temperatures and apply an experimentally determined version of C_{tbl} that we will call C_T:

$$C_T = \frac{\text{isothermal wall }(T)}{\text{isothermal wall }(T_{\mathrm{ref}})}=\frac{C_{\mathrm{tbl}}(T_{\mathrm{wall}})}{C_{\mathrm{tbl}}(T_{\mathrm{ref}})}=1+K_T\,Re^{-1/2}\left[\frac{\Delta T}{T_0}\right] \tag{12}$$

Although C_{tbl} and C_T are closely related, they are not the same quantity. As defined in Equation (9), C_{tbl} accounts for the change in the mass flow caused by the thermal boundary layer between the adiabatic wall condition and a non-adiabatic, isothermal wall at T_{wall}. The quantity C_T accounts for the change in mass flow caused by the thermal boundary layer, under non-adiabatic and isothermal wall conditions, when the wall is at T_{wall} versus a reference temperature T_{ref}. The subscript on coefficient K_T in Equation (12) indicates that K_T: (1) is used to calculate C_T, (2) may differ from the theoretical K_{tbl}, and (3) is determined experimentally. Like C_{tbl}, C_T is dependent on the gas species via γ.

5. Temperature distributions in the bodies of CFVs

We conducted thermal boundary layer measurements using heated CFVs made of stainless steel, copper, and a machinable ceramic (Macor[3]). For the copper CFVs, the thermal resistance between the CFV wall and the gas flow is much greater than the thermal resistance of the copper body; therefore, the temperature anywhere within the CFV body is a good approximation to the temperature of the inner wall of the CFV (See Fig. 4.). Section 5.1 describes a finite-volume numerical model used to estimate the temperature profile in the CFV. Section 5.2 provides a simple analytical model for the temperature profile and Section 5.3 discusses both predicted radial temperature profiles.

5.1. Computational model

A computational fluid dynamics (CFD) code (Fluent™) was used to calculate the temperature distribution of the gas flowing through the CFV at the maximum tested pressure (700 kPa). The CFD solution was coupled to CFV bodies with T_{surf} = 313 K made of 1) copper-tellurium alloy (Cu), 2) 316 stainless steel (SS), and 3) ceramic materials to compute the temperature distribution within the CFV bodies. Laminar flow conditions were assumed for the gas flow simulation and the ends of the CFV bodies were adiabatic. Fig. 4 shows pictures of some of the CFVs tested and the computed temperature distributions for d = 3.2 mm CFVs made of the three materials. The temperature distributions in the diverging sections of the CFVs are difficult to predict because they depend on the position of shock waves. We do not expect the CFD simulations to accurately capture the positions of shocks and other details of the flow, but they do give qualitative temperature distributions for the bodies of the CFVs. Note that the CFV wall temperature varies along the flow path, but the bodies of the metal CFVs are nearly isothermal for the more conductive materials. The temperature of the CFV wall upstream from the throat determines the significance of the thermal boundary layer effects.

5.2. Analytical model

The analytical temperature model assumed 1-dimensional, isentropic, over-expanded (no shocks) flow to calculate the adiabatic wall temperature [2] through an ISO toroidal CFV. We assumed a constant temperature for the CFV exterior surface. We used Smith and Spalding's [24] convective heat transfer coefficient for the boundary layer and a textbook heat transfer model for cylindrical shells [23] to calculate the temperature on the CFV interior wall. To simplify calculation of the temperature distribution in the CFVs, we assumed no heat transfer in the axial direction.

Fig. 5 shows temperatures from the analytical model for a CFV made of stainless steel with 17.5 mm body radius and a throat diameter d =

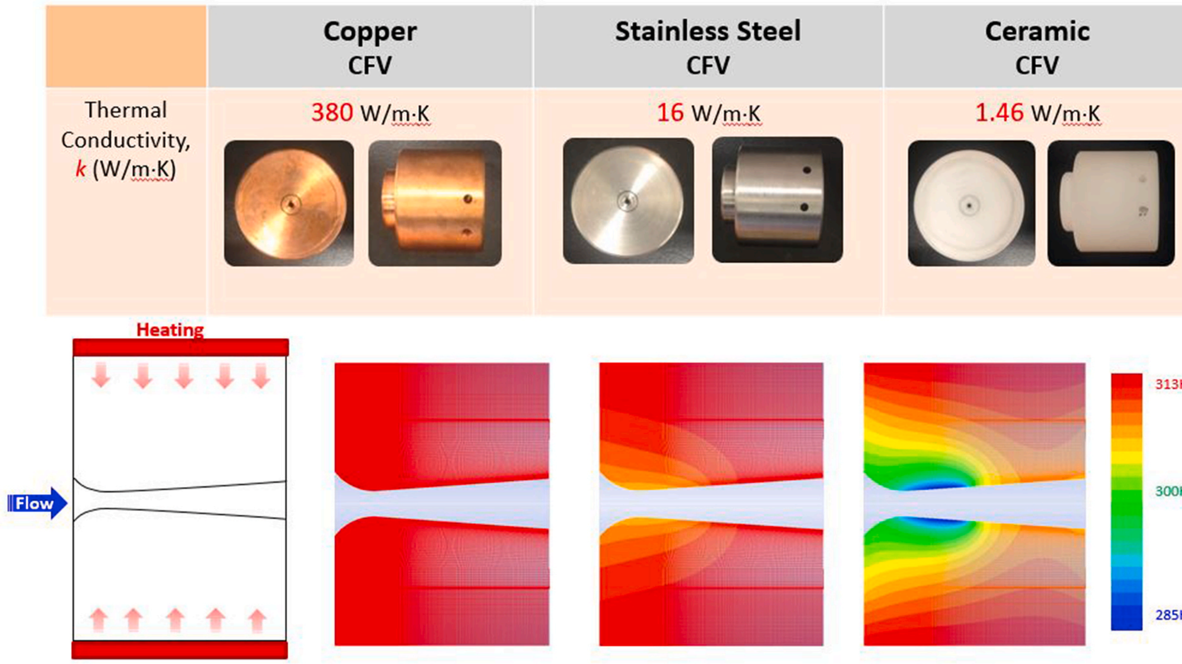

Fig. 4. Temperature distribution within the CFV body from the computational model for the d = 3.2 mm CFVs made of three materials at stagnation pressure of 700 kPa.

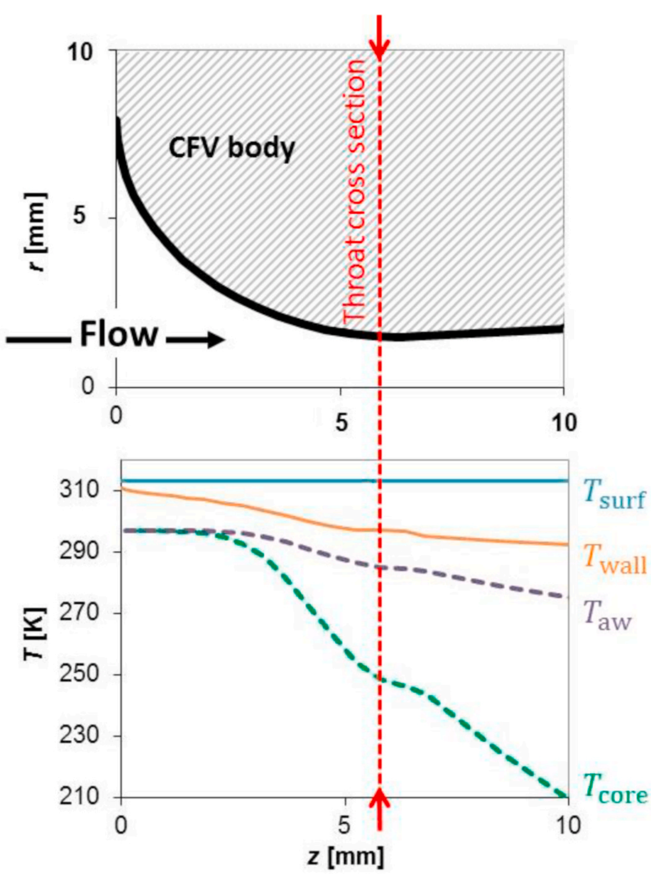

Fig. 5. Analytically modeled radial temperature profile for an externally heated (T_{surf} = 313 K) d = 3.2 mm stainless steel CFV.

3.2 mm. Fig. 5 shows temperatures on a plane bisecting the CFV in the axial direction; 1) the heated CFV exterior T_{surf} = 313 K, 2) the temperature of the CFV interior wall T_{wall}, 3) the adiabatic wall temperature T_{aw} , and 4) the temperature of the gas in the free stream T_{core}. The adiabatic wall temperature is warmer than the core flow due to viscous heating in the boundary layer. The temperatures predicted by the analytical model in the radial direction at the throat cross section will be discussed in the following section along with the results from the finite-volume computational model.

5.3. Radial temperature distribution

Fig. 6a and b shows temperature profiles for radial sections at the CFV throat for a $d = 3.2$ mm and a $d = 0.56$ mm CFV respectively, for all three CFV body materials. The results from the analytical model are shown as symbols and the computational model results are shown as solid lines. The two models for the temperature in the CFV body agree within 1.2 K.

Fig. 6 illustrates the importance of the Biot number in the thermal boundary layer experiments. The Biot number is the ratio of the resistance to conductive heat transfer inside the CFV body to the convective heat transfer resistance at the surface: $Bi = h\ell/k$ where h is the convective heat transfer coefficient of the gas flowing inside the CFV, ℓ is a characteristic length of the CFV (the distance between the interior and exterior CFV walls), and k is the thermal conductivity of the CFV material. When the CFV thermal conductivity is larger (as is true for copper relative to stainless steel or ceramic), the Biot number is lower, and the CFV body temperature is nearly uniform and equal to the external, controlled temperature. Conversely, a larger Biot number leads to a larger temperature gradient in the CFV body. A larger flow (larger h) or less conductive CFV material will cause a larger Biot number. If we design a CFV with low Biot number, a temperature measurement made anywhere within the CFV body will be a good approximation of the CFV interior wall temperature T_{wall}.

In our measurements using copper and stainless steel CFVs (Section 6), we inferred T_{body} and T_{wall} from the temperature measured by a bead thermistor embedded in the CFV body 5.5 mm from the CFV centerline

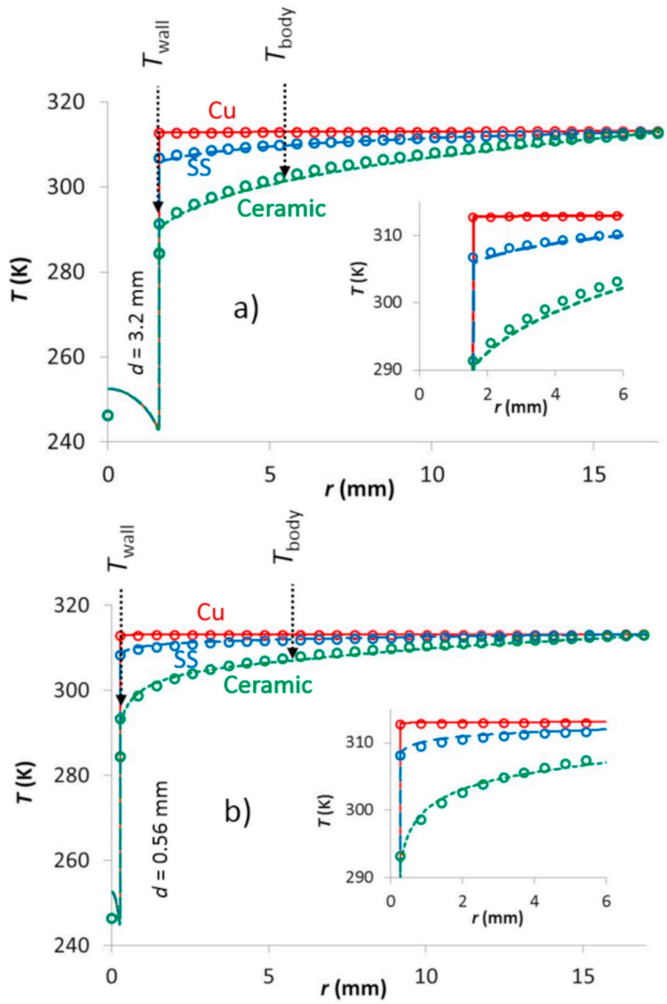

Fig. 6. Radial temperature distributions at the CFV throat, copper, stainless steel (SS), and ceramic materials, for the a) $d = 3.2$ mm and b) $d = 0.56$ mm CFVs. Lines are from the computational model and symbols are from the analytical model. The inserts show the near wall region with higher resolution.

(This position is indicated by T_{body} in Fig. 6.). Both thermal models indicate that $T_{body} - T_{wall} < 0.2$ K for the copper CFVs and <3.9 K for the stainless steel CFVs. However, T_{body} is a poor approximation of T_{wall} for the ceramic material: $T_{body} - T_{wall}$ is as large as 15 K. Ceramic is a good insulator and more closely approximates the adiabatic wall condition used in theoretical calculations of the discharge coefficient.

6. Experimental measurement of C_T

The goal of the CFV holder and approach-pipe design was to accurately measure the gas temperature entering a CFV with an elevated body temperature. CFVs with $d = 3.2$ mm, 1.1 mm, and 0.56 mm were machined from copper, stainless steel, and a machinable ceramic material. The 9 CFVs were calibrated against the NIST *PVTt* flow standards [19] using an experimental arrangement designed to minimize temperature sampling errors. The temperature of the CFV body was proportional-integral-derivative (PID) controlled at four set points by an electric heater to measure the influence of the thermal boundary layer on the CFV discharge coefficients.

Some features of the experimental design are:

1) Thermostatted water was pumped through a plate heat exchanger to condition the incoming gas to match the nominal room temperature (296.7 K), thereby minimizing heat transfer from the room through the approach-pipe walls. The CFV inlet gas temperatures were 297 K ± 0.7 K during tests. The room temperature measured by a thermistor 1 m away from the test section was always in the interval 297 K ± 0.3 K.
2) Each CFV was installed between inlet and outlet pipes made of fiberglass-filled PTFE with O-ring seals (see Fig. 8). Relative to stainless steel approach pipes, the PTFE had 1/60th of the thermal conductivity and 3.7 times the cross-sectional area. Therefore, replacing steel with PTFE reduced the heat flux on path 2 in Fig. 2 by a factor of 16.
3) To measure streamwise temperature changes as the gas approached the CFV entrance, we inserted two thermistors (T_1 and T_2 in Fig. 8) through the wall of the approach pipe. These thermistors were axially displaced from the CFV entrance plane by 40 mm (T_1) and 73 mm (T_2). Each thermistor had a 3 mm diameter stainless steel sheath. Nylon compression fittings reduced stem conduction errors (path 3 in Fig. 2). To measure the gas temperature close to the CFV entrance plane with negligible stem-conduction errors, we installed a 1.25 mm exposed bead thermistor (T_z in Fig. 8) on the approach-pipe centerline. This thermistor had a large (>300 mm) immersion depth. To position the T_z sensor as close to the CFV entrance plane as practical, we measured $\dot{m}_{ref}/\dot{m}_{CFV}$ at a constant flow while we moved the sensor incrementally closer to the CFV entrance plane. At the largest flow (3.2 mm CFV, 700 kPa), the T_z sensor altered $\dot{m}_{ref}/\dot{m}_{CFV}$ measurements by less than 0.02 % when it was located 10 mm from the entrance plane. For all the measurements in this study, the T_z measurements were made at that 10 mm position and the three gas temperature measurements, T_1, T_2, and T_z agreed with each other within 0.3 K. A temperature uncertainty of 0.3 K propagates into a 0.05 % uncertainty in $\dot{m}_{ref}/\dot{m}_{CFV}$ measurements

Two temperature sensors were inserted in oil-filled thermowells drilled into the CFV body (see Figs. 7 and 8). One temperature sensor was used as the input to a PID controlled heater to maintain the CFV at the desired T_{body} set points. The other sensor was an exposed bead thermistor to measure T_{body}. Both thermowells reached within 5.5 mm of the CFV centerline. A thin film 1.5 mm × 1.5 mm temperature sensor was taped to the exterior surface of the CFV body (T_{surf}), but the surface temperature measurements had large uncertainty.

Each of the 9 CFVs was calibrated with dry air (dew point temperature of 256 K) at 6 pressure setpoints (200 kPa–700 kPa in 100 kPa increments). The discharge coefficient of the CFV was measured with a $k = 2$ uncertainty of 0.06 %,. The PID temperature controller and an electric heater wrapped around the CFV exterior were used to control T_{body} to nominal values of 298 K, 303 K, 308 K, and 313 K ± 0.9 K.

Three or more 34 L or 677 L *PVTt* collections were made at each pressure set point. Each *PVTt* flow collection (and averages of other sensor measurements) lasted between 0.3 min and 30 min. The data acquisition system also logged temperature and pressure measurements from numerous sensors at 10 s intervals.

7. Analysis of experimental results

The calibration data consisted of the reference mass flow from the *PVTt* standard, the composition of the dried air, the static pressure (P_0) and temperature upstream (T_0 based on T_z) from the CFV, and the temperature of the CFV body. The corrections from static to stagnation pressure were all small (<0.012 %) because the ratio of the approach-pipe and throat diameters was >6 for these experiments.

The mass flow calculated via the CFV, accounting for thermal expansion of the CFV material is $\dot{m}_{R*,\alpha} = C_\alpha \dot{m}_{R*}$ and experimental values of this quantity for the three copper CFVs are plotted versus $Re^{-1/2}$ in Fig. 9.

The throat area at the reference temperature was calculated by fitting $\dot{m}_{ref}/\dot{m}_{R*}$ results for CFV body temperature of ≈298.15 K to

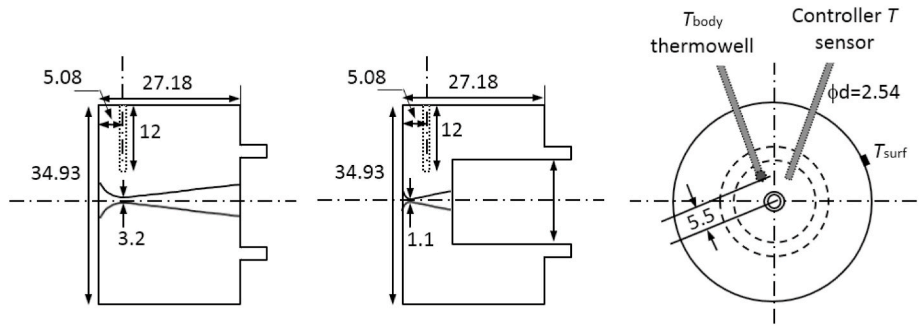

Fig. 7. Construction details and locations of CFV temperature sensors for the 3.2 mm and 1.1 mm CFVs (all dimensions in mm).

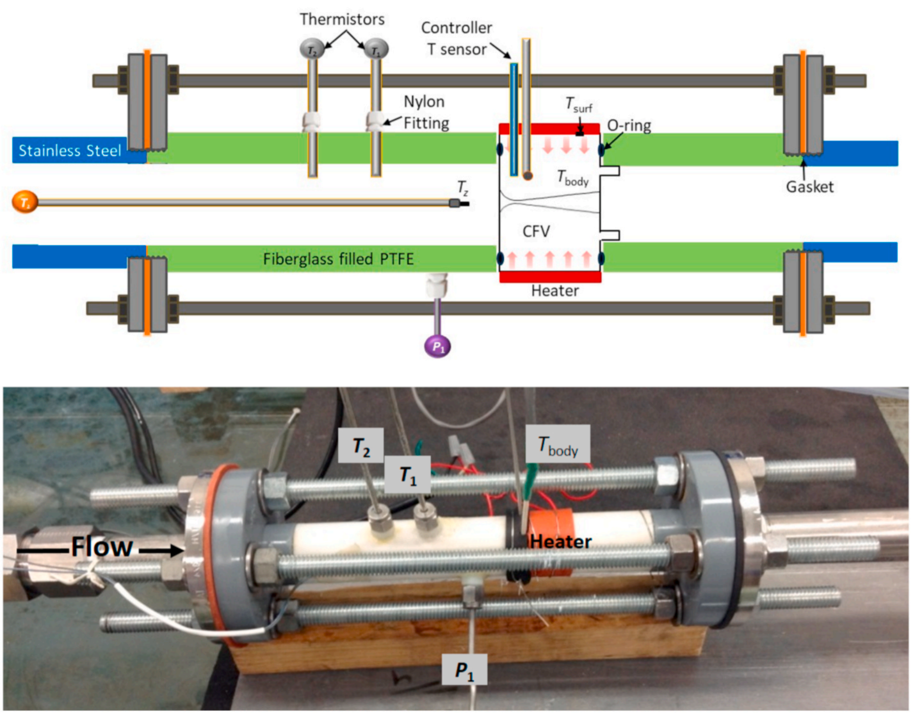

Fig. 8. Experimental arrangement and locations of sensors.

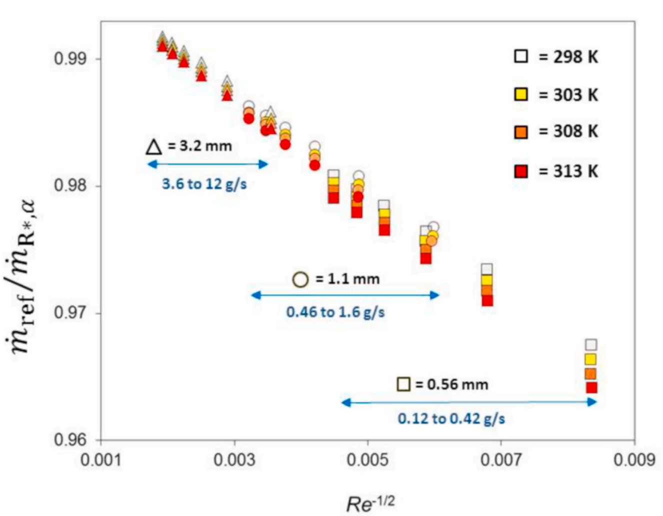

Fig. 9. Discharge coefficient $\dot{m}_{ref}/\dot{m}_{R*,\alpha}$ for the three copper CFVs at body temperatures of 298 K, 303 K, 308 K, and 313 K.

analytical $C_{inv}C_{vbl}$ values based on Geropp [8] and Kleigel and Levine [6]. This fitting gave throat diameter and inlet curvature ratio Ω values that would be difficult to obtain by dimensional metrology because of the small size of the CFVs. However, this fit to obtain d_{ref} values was not critical: nominal values of d_{ref} give insignificantly different results for the experimental C_T values. Fig. 9 plots the discharge coefficient with thermal expansion corrections ($\dot{m}_{ref}/\dot{m}_{R*,\alpha}$) for the three copper CFVs at four CFV body temperatures. The discharge coefficient $\dot{m}_{ref}/\dot{m}_{R*,\alpha}$ decreases with increasing body temperature and the effect is more pronounced for smaller Reynolds number.

For each CFV, the $\dot{m}_{ref}/\dot{m}_{R*,\alpha}$ values for the $T_{body} = T_{ref} = 298.15$ K data set were fitted by a 3rd order polynomial of $Re^{-1/2}$. The 3rd order fit and calibration data collected at $T_{body} = 298$ K, 303 K, 308 K, and 313 K were used to calculate a thermal boundary layer correction from the calibration data:

$$C_T \cong \frac{\left[\dot{m}_{ref}/\dot{m}_{R*,\alpha}\right]_{T_{body}}}{\left[\dot{m}_{ref}/\dot{m}_{R*,\alpha}\right]_{T_{ref}}} \cong 1 + \left(\left[\frac{\dot{m}_{ref}}{\dot{m}_{R*,\alpha}}\right]_{T_{body}} - \left[\frac{\dot{m}_{ref}}{\dot{m}_{R*,\alpha}}\right]_{T_{ref}}\right) \quad (13)$$

Note that $\dot{m}_{ref}/\dot{m}_{R*,\alpha}$ is equivalent to an experimental measurement of

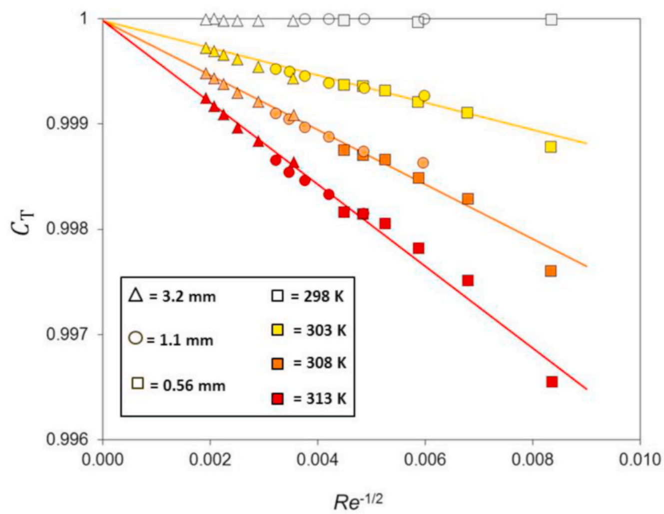

Fig. 10. for various throat diameters and body temperatures plotted versus $Re^{-1/2}$ using the same data as in Fig. 9.

$C_{inv}C_{vbl}C_{tbl}$ (often called C_d) and C_T corrects for changes in the CFV mass flow for various values of T_{body} (or T_{wall}) relative to the mass flow through the CFV at the reference temperature.

Fig. 10 plots values of C_T calculated from Equation (13) using the same data presented in Fig. 9. For each nominal T_{body} set point, a linear function of $Re^{-1/2}$ fits the results for three different throat diameter CFVs within ±0.0002.

A plot of C_T calculated from experimental data via Equation (13) versus $Re^{-1/2}(\Delta T)/T_0$ for the copper CFVs is shown in Fig. 11. The slope of the data in Fig. 11 (K_T) and Equation (12) can be used to calculate C_T when the CFV is used to measure flow under some new temperature condition. The value of K_T measured in these experiments (excluding the 3.2 mm stainless steel CFV) was −7.15, while Geropp's theoretical value of K_{tbl} for air and a CFV of standard geometry is −1.7 and Ding *et* al. found K_{tbl} = -3.845.

Results for the three stainless steel CFVs are shown in Fig. 12. The offset in the 3.2 mm data relative to the other two CFVs is likely due to increasing differences between T_{body} and T_{wall} for this particular CFV because the Biot number is large: 1) the 3.2 mm CFV produces the

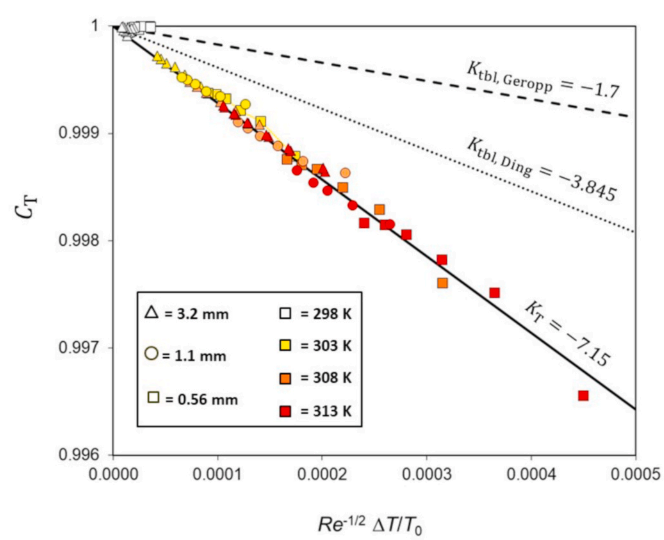

Fig. 11. versus $Re^{-1/2}(\Delta T)/T_0$ for the copper CFVs using the same data in Figs. 9 and 10. The dashed lines represent the theoretical values of Geropp ($K_{tbl,\ Geropp} = -1.7$) and Ding et al. ($K_{tbl,\ Ding} = -3.845$).

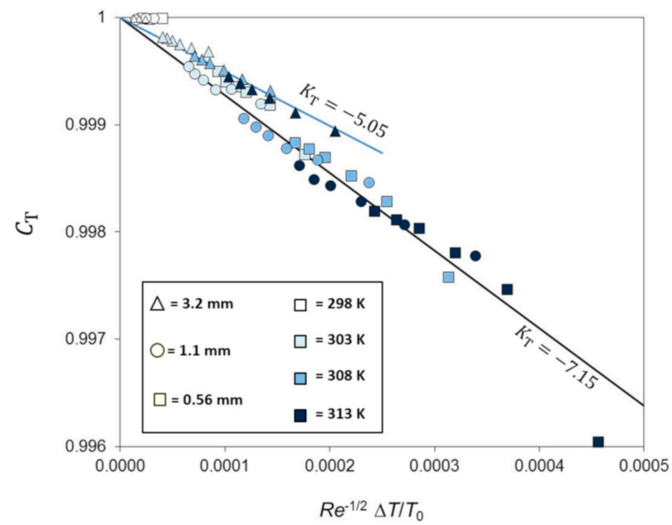

Fig. 12. versus $Re^{-1/2}(\Delta T)/T_0$ for the stainless steel CFVs.

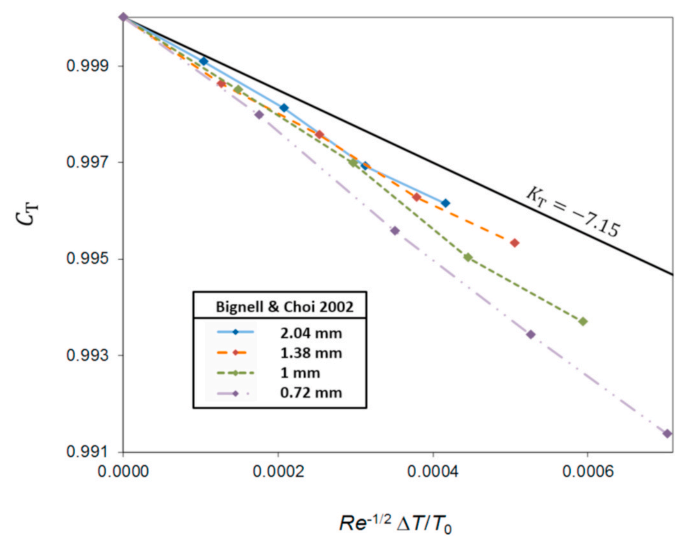

Fig. 13. Bignell and Choi's experimental results for C_T and the slope K_T of results from this work.

largest flows and hence the greatest heat flux from the CFV body into the flowing gas and 2) stainless steel is less thermally conductive than copper. Although T_{body} is controlled, the controller temperature sensor is displaced from the wall and the temperature gradient is significant. This leads to T_{wall} being several degrees cooler than T_{body} and a measured value of C_T that is closer to unity. Ignoring the 3.2 mm data, the slope (K_T) of the stainless steel data in Fig. 12 and the copper data in Fig. 11 is −7.15. The slope for the 3.2 mm stainless steel CFV data is −5.05.

8. Discussion and conclusions

Temperature sampling errors are the largest concern when trying to achieve CFV flow measurements that are reproducible under variable room temperature or gas temperature conditions. The gas expanding through the CFV cools the CFV body and connecting piping which causes temperature gradients in the gas and can lead to stem conduction errors in the gas temperature sensor. In these experiments, a special design improved the measurement of T_0. Improved designs for measuring the temperature of gas in commercially applied CFVs are needed.

Mass flow through a CFV is predictably sensitive to the temperature of the CFV body, and thermal effects can be corrected via the equation:

$$\dot{m}_{\mathrm{CFV}} = [C_{\mathrm{inv}}C_{\mathrm{vbl}}C_{\mathrm{tbl}}]_{T_{\mathrm{ref}}} C_{\alpha} C_{\mathrm{T}} C_{\mathrm{R}}^{*} \frac{P_0 A_{\mathrm{ref}} \sqrt{M}}{\sqrt{RT_0}} \tag{14}$$

where $[C_{\mathrm{inv}}C_{\mathrm{vbl}}C_{\mathrm{tbl}}]_{T_{\mathrm{ref}}}$ represents what most CFV users call the discharge coefficient (C_{d}), measured experimentally while the CFV body is maintained at a reference temperature, C_{α} corrects for thermal expansion of the CFV material relative to the reference temperature, and C_{T} corrects for thermal boundary layer effects relative to the reference temperature. The remainder of Equation (14) is what we call herein the 0^{th} order CFV model.

The thermal boundary layer correction C_{T} is determined experimentally by calibrating the CFV at various body temperatures T_{body} to determine the value of K_{T} that is used in Equation (12): $C_{\mathrm{T}} = 1 + K_{\mathrm{T}} Re^{-1/2}[\Delta T/T_0]$ where ΔT is $T_{\mathrm{wall}} - T_0$. For low Biot numbers, $T_{\mathrm{body}} \approx T_{\mathrm{wall}}$. A practical approach to applying the results of this paper is to use a thermally conductive CFV material, control the heat transfer paths shown in Fig. 2, measure T_{body} in the configuration that is to be used later, and apply Equation (12). Fig. 1 illustrates that for a $d = 0.56$ mm CFV subjected to a 7 K room temperature change, an order of magnitude reduction in flow errors is possible this way: under steady state temperature conditions, the temperature effects without C_{T} applied were 0.02 % K^{-1}, but with C_{T} applied, the effects were reduced to a negligible level.

The nearly linear dependence of C_{T} on $Re^{-1/2}[\Delta T/T_0]$ is predicted by Geropp's 1987 paper and is demonstrated by the experimental results for CFVs of three throat diameters, two materials, at four body temperatures shown in Figs. 11 and 12. Unfortunately, the theoretical K_{tbl} values of Geropp (−1.7), Ding et al. (−3.845), and our experimental value of K_{T} (-7.15) are quite different. We observe that values of K_{T} (and for the y-axis intercept) for various installation configurations (i.e. materials, insulation, external temperature conditions, boundary conditions) are likely to differ. For example, the value of K_{T} used in Fig. 1 was −11.5, rather than the value −7.15 measured during the controlled CFV body temperature experiments. Bignel and Choi's measured K_{T} as small as −12.3.

The non-adiabatic condition of the nozzle wall is not only a consequence of heated or cooled nozzle bodies but also a consequence of the Prandtl numbers of real gases differing from unity. Recent comparison between experimental and numerical results [25] obtained with air ($Pr = 0.72$) for small stainless steel nozzles demonstrated that the agreement between predictions of $C_{\mathrm{inv}}C_{\mathrm{vbl}}C_{\mathrm{tbl}}$ using the solutions of Geropp, Kliegel, and Levine are reasonable for usual environmental conditions in a laboratory but there is a significant disagreement if Argon ($Pr = 0.67$) is used; therefore, a simple transformation of results gathered with a reference gas (e.g. air or nitrogen) to a different gas (with different Prandtl number) might be possible. Until this is demonstrated, the empirical correction factor C_{T} should be experimentally measured for the particular gas in which the CFV will be applied.

Possible explanations for the difference between our experimental and the theoretical values are 1) the different reference conditions used for C_{tbl} and C_{T} (adiabatic wall and T_{ref} respectively), 2) a curvature ratio Ω much smaller than the 0.25 that we used, and 3) the isothermal CFV wall assumed in the theoretical analyses does not match experimental conditions. Note that temperature sampling errors are an unlikely explanation: the most likely temperature sampling error would lead to an incorrectly low measurement of T_0 which would worsen the agreement between K_{T} and K_{tbl}. Until the reasons for the difference between theory and experiments is understood and controlled, it will be necessary to measure K_{T} for each CFV design, but we note that Equation (12) fits well for various CFV installation configurations.

Obtaining a good estimate of T_{wall} is necessary for making thermal effect corrections. In our case, a thermowell in the CFV body and a bead thermistor were used to measure T_{body} and we assumed that $T_{\mathrm{body}} \approx T_{\mathrm{wall}}$. For small throat diameter CFVs made of conductive CFV material (copper or stainless steel), this works well. We know that the difference between the measured T_{body} and T_{wall} grows with the Biot number (decreasing thermal conductivity of the CFV material or increasing Reynolds number or flow). Better estimates of T_{wall} can be made by making two temperature measurements at precisely known depths in the CFV body and using the expected logarithmic relationship between radial depth versus temperature to calculate extrapolated values of T_{wall}.

Constructing the CFV from a material with low thermal conductivity (i.e. ceramic) leads to a large Biot number, more closely approximates the adiabatic wall used in analytical C_{vbl} calculations, and reduces the influence of thermal boundary layers on the mass flow. We constructed CFVs from a machinable ceramic material that has thermal conductivity of 1.46 W/m-K. Unlike the copper or stainless steel CFVs, the low thermal conductivity of ceramic means that the CFV body temperature measured in the thermowell is not a good approximation of the wall temperature ($T_{\mathrm{body}} - T_{\mathrm{wall}}$ was as large as 15 K for our ceramic design). To make the comparisons more consistent, the CFVs made of Cu, stainless steel, and ceramic were tested with controlled external surface temperatures using an electric heater and a 1.5 mm × 1.5 mm thin film temperature sensor placed between the CFV surface and the electric heater. Even with thermally conductive grease between the CFV and the heater, it is difficult to acquire low uncertainty surface temperature measurements and the results of these tests are not as clear as when the CFV body temperature was controlled. But the sensitivity of the CFV mass flow to the surface temperature changes was approximately 30 % smaller for the ceramic CFVs than for the metal CFVs.

Bignell and Choi [18] calibrated four heated CFVs and we have used Fig. 6 in their publication to calculate C_{T} values. Their results are plotted in Fig. 13. The decrease in flow as the CFV body temperature is raised is similar to our results for their largest two CFVs, but thermal effects are larger for the smaller CFVs and are not a linear function of $Re^{-1/2}$. We also observed similar (but less pronounced) nonlinear effects in our data at large values of $Re^{-1/2}$ (corresponding to low values of Re). Perhaps at low Re, the residence time of the gas near the CFV entrance plane is long enough that heat conduction from the hot CFV body through the gas is causing errors in the measurement of T_0. Note that if the actual T_0 is higher than the measured value, smaller experimental values of C_{T} will result.

It is worth noting that if one controls T_{body} and T_0 when a CFV is calibrated and used, effects due to C_{α} and C_{T} are constant for a particular flow and gas species. Hence a practical approach to improving the reproducibility of measurements with small CFVs is to control the CFV body, approach-pipe, and gas temperatures with PID controlled Peltier effect heaters/coolers and use the same temperature set points during calibration and usage.

Author statement

John Wright: conceptualization, methodology, software, validation, formal analysis, investigation, writing -original draft, writing – Review and editing, visualization, supervision, Woong Kang: software, validation, formal analysis, investigation, writing – Review and editing, visualization, Aaron Johnson: formal analysis, investigation, software, writing – Review and editing, Vladimir Khromchenko: software, validation, formal analysis, investigation, Michael Moldover: methodology, formal analysis, writing – Review and editing, visualization, Liang Zhang: software, validation, formal analysis, investigation, Bodo Mickan: software, formal analysis, writing – Review and editing.

Declaration of competing interest

The authors declare that they have no known competing financial interests or personal relationships that could have appeared to influence the work reported in this paper.

Acknowledgements

This work was partially supported by a Cooperative Research and Development Agreement with WEST, Inc. and their subsidiary Flow Systems, Inc. We also wish to acknowledge Gina Kline of the NIST Fluid Metrology Group for her assistance in the laboratory. This research did not receive any specific grant from funding agencies in the public, commercial, or not-for-profit sectors.

References

[1] E.W. Lemmon, M.L. Huber, M.O. McLinden, NIST Standard Reference Database 23: Reference Fluid Thermodynamic and Transport Properties-REFPROP, National Institute of Standards and Technology, Standard Reference Data Program, Gaithersburg, 2007, Version 9.0.

[2] J.D. Anderson, Modern Compressible Flow, third ed., McGraw Hill, 2004.

[3] International Standards Organization, Measurement of gas flow by means of critical flow venturi nozzles, second ed., ISO 9300, 2005.

[4] American Society of Mechanical Engineers, Measurement of gas flow by means of critical flow venturis and critical flow nozzles, 2016. ASME MFC-7-2016.

[5] G.W. Hall, Transonic flow in two-dimensional and axially-symmetric nozzles, Quart, J. Mech. Appl. Math. 15 (1962) 487–508.

[6] J.R. Kliegel, J.N. Levine, Transonic flow in small throat radius of curvature nozzles, AIAA J. 7 (1969) 1375–1378.

[7] S.P. Tang, Discharge coefficients for critical flow nozzles and their dependence on Reynolds number, Ph. D. Thesis Princeton University, 1969. Princeton, New Jersey, USA.

[8] D. Geropp, Laminare Grenzschichten in Ebenen und Rotationssymmetrischen Lavaldusen, Deutsche Luft- und Raumfahrt Forschungsbericht 71 – 90, 1971.

[9] A.N. Johnson, J.D. Wright, Comparison between theoretical CFV models and NIST's primary flow data in the laminar, turbulent, and transition flow regimes, ASME J. Fluid. Eng. 130 (July, 2008).

[10] M. Ishibashi, T. Morioka, B.T. Arnberg, Effect of inlet curvature on the discharge coefficients of toroidal-throat critical-flow venturi nozzles, fedsm2005–77470, in: Proceedings of the ASME Fluids Engineering Summer Meeting, 2005. Houston, Texas, USA.

[11] B. Mickan, R. Kramer, D. Dopheide, Determination of discharge coefficient of critical nozzles based on their geometry and the theory of laminar and turbulent boundary layers, in: Proceedings of the 6th International Symposium on Fluid Flow Measurement, Queretaro, Mexico, May, 2006.

[12] B. Mickan, R. Kramer, D. Dopheide, H.-J. Hotze, H.-M. Hinze, A.N. Johnson, J. D. Wright, J.-P. Vallet, Comparisons by ptb, NIST, and LNE-LADG in air and natural gas with critical venturi nozzles agree within 0.05 %, comparisons by ptb, NIST, and LNE-LADG IN air and natural gas with critical venturi nozzles agree within 0.05 %, in: Proceedings of the 6th International Symposium on Fluid Flow Measurement, Queretaro, Mexico, May, 2006.

[13] J.D. Wright, W. Kang, L. Zhang, A.N. Johnson, M.R. Moldover, Thermal effects on critical flow venturis, in: Proceedings of the 9th International Symposium on Fluid Flow Measurement, 2015. Arlington, Va, USA, April 14 to 17.

[14] J.D. Wright, Uncertainty of the critical venturi transfer standard used in the K6 gas flow key comparison, in: Proceedings of FLOMEKO, 2007. Johannesburg, South Africa.

[15] E.H. Jones, Material temperature profiles in a critical flow nozzle, in: ASME Winter Annual Meeting, Nov. 27 to Dec. 2, 1988. Chicago, Illinois, USA.

[16] R.W. Caron, M.S. Carter, Temperature profile within sonic nozzles, in: 3rd International Symposium on Fluid Flow Measurement, 1995. San Antonio, Texas, USA.

[17] T.M. Kegel, R.W. Caron, Some effects of thermal phenomena on the accuracy of CFV based flowrate measurements, in: Proceedings of the ASME Fluids Engineering Summer Meeting, 1996. San Diego, California, USA.

[18] N. Bignell, Y.M. Choi, Thermal effects in small sonic nozzles, Flow Meas. Instrum. 13 (2002) 17–22.

[19] J.D. Wright, A.N. Johnson, M.R. Moldover, G.M. Kline, Gas flowmeter calibrations with the 34 L and 677 L PVTt standards, in: NIST Special Publication 250–63, National Institute of Standards and Technology, Gaithersburg, Maryland, 2010. November 18.

[20] H.-B. Ding, C. Wang, G. Wang, Thermal effect on mass flow-rate of sonic nozzle, Therm. Sci. 22 (2018) 247–262.

[21] J.G. Pope, J.D. Wright, Performance of coriolis meters in transient gas flows, Flow Meas. Instrum. 37 (2014) 42–53.

[22] D. Geropp, *Grenzschichten in Uberschalldusen*, Deutsche Luft- und Raumfahrt Forschungsbericht 01 TM 8603-AK/PA 1, 1987.

[23] A. Bejan, Heat Transfer, Section 2.2, John Wiley and Sons, 1993.

[24] A.G. Smith, D.B. Spalding, Heat transfer in a laminar boundary layer with constant fluid properties and constant wall temperature, J. Royal Aero. Soc. 62 (1958) 60–64.

[25] B. Mickan, C.-Y. Kuo, M. Xu, Systematic investigations of cylindrical nozzles acc. ISO 9300 down to throat diameters of 125 μm, in: Proceedings of the 10th International Symposium on Fluid Flow Measurement, March, 2018. Queretaro, Mexico.